

PAPER

Pressure-induced superconductivity in palladium sulfide

To cite this article: Liu-Cheng Chen *et al* 2018 *J. Phys.: Condens. Matter* **30** 155703

View the [article online](#) for updates and enhancements.

Related content

- [Superconductivity in alkali metal intercalated iron selenides](#)
A Krzton-Maziopa, V Svitlyk, E Pomjakushina *et al*.
- [Effects of pressure and distortion on superconductivity in \$Tl_2Ba_2CaCu_2O_{8+x}\$](#)
Jian-Bo Zhang, Viktor V Struzhkin, Wenge Yang *et al*.
- [Structural and optical investigations of \$Fe_{1.03}Se_{0.5}Te_{0.5}\$ under high pressure](#)
Pallavi S Malavi, S Karmakar, N N Patel *et al*.

Pressure-induced superconductivity in palladium sulfide

HPSTAR
550-2018

Liu-Cheng Chen^{1,2,3} , Hao Yu³, Hong-Jie Pang³, Bin-Bin Jiang^{4,5}, Lei Su⁶, Xun Shi⁴, Li-Dong Chen⁴ and Xiao-Jia Chen³

¹ Key Laboratory of Materials Physics, Institute of Solid State Physics, Chinese Academy of Sciences, Hefei 230031, People's Republic of China

² University of Science and Technology of China, Hefei 230026, People's Republic of China

³ Center for High Pressure Science and Technology Advanced Research, Shanghai 201203, People's Republic of China

⁴ State Key Laboratory of High Performance Ceramics and Superfine Microstructure, Shanghai Institute of Ceramics, Chinese Academy of Science, Shanghai 200050, People's Republic of China

⁵ University of Chinese Academy of Sciences, Beijing 100049, People's Republic of China

⁶ Key laboratory of Photochemistry, Institute of Chemistry, University of Chinese Academy of Sciences, Chinese Academy of Sciences, Beijing 100190, People's Republic of China

E-mail: xjchen@hpstar.ac.cn

Received 2 February 2018, revised 5 March 2018

Accepted for publication 9 March 2018

Published 22 March 2018



Abstract

An extended study on PdS is carried out with the measurements of the resistivity, Hall coefficient, Raman scattering, and x-ray diffraction at high pressures up to 42.3 GPa. With increasing pressure, superconductivity is observed accompanying with a structural phase transition at around 19.5 GPa. The coexistence of semiconducting and metallic phases observed at normal state is examined by the Raman scattering and x-ray diffraction between 19.5 and 29.5 GPa. After that, only the metallic normal state maintains with an almost constant superconducting transition temperature. The similar evolution between the superconducting transition temperature and carrier concentration with pressure supports the phonon-mediated superconductivity in this material. These results highlight the important role of pressure played in inducing superconductivity from these narrow band-gap semiconductors.

Keywords: transition metal chalcogenides, superconductivity, pressure effect, Raman spectrum

(Some figures may appear in colour only in the online journal)

1. Introduction

Since the discovery of LaFeAsO_{1-x}F_x superconductor, various Fe-based superconductors have been synthesized with the motivation to enhance superconducting transition temperature (T_c) [1–4]. Among them, iron-based chalcogenides have been of great interest because of their fascinating superconducting properties [5–9]. For example, FeSe is regarded as a reference material to elucidate the physics of high T_c superconductivity in Fe-based compounds, due to the simplest crystallographic structure [10–13]. Pressure is a clean tool to find new superconductors or enhance the properties of existing superconductors without inducing impurities. The T_c of FeSe is 8 K at ambient pressure, and increases to 36.7 K

under external pressure [14, 15]. Although FeSe system possesses many attractive features, lots of physical properties still remain unsettled. For example, FeSe_{1-x} always composes of primarily PbO-type tetragonal phase with space group $P4/nmm$ and NiAs-type hexagonal phase with space group of $P6_3/mmc$ [14]. At low temperatures, a structural transition from $P4/nmm$ to an orthorhombic phase with space group was reported from neutron diffraction measurements [23]. The central issue regarding which phase(s) accounts for superconductivity remains unknown. At high pressures, the T_c evolution paths detected from different groups are very different [15, 24–27]. There has been no agreement about the high-pressure structures and phase transformation for this so-called simple material [15, 24, 28, 29]. It has been generally accepted

[30] that applied pressure enhances spin fluctuations and thus T_c in Fe_{1+x}Se , suggesting a close linkage between spin fluctuations and the mechanism of superconductivity. This seemingly beautiful picture does not get further support from the direct detection of magnetic excitations from neutron scattering measurements [31]. The spin resonance energy was not observed to be proportional to T_c at high pressures [31]. This indicated that pairing beyond magnetic excitations should account or at least work together with for superconductivity in FeSe. On the other hand, the strong pressure-dependent electron–phonon coupling was suggested from theoretical study on FeSe [32]. The newly developed techniques based on photoemission and x-ray free electron laser were used to determine the weight of interactions. The new experiment confirmed the theoretically predicted enhancement of the electron–phonon coupling strength owing to electron–electron correction effects [33]. The sister compound FeS has also attracted great interest due to the comparability with FeSe [16, 17]. Superconductivity in tetragonal FeS was observed with a T_c of 5 K, but T_c gradually decreases with pressure, contrary to the case in FeSe [18, 19]. Although there has been no report of superconductivity in the undoped FeTe, the extensive studies on FeTe system have promoted the understanding of superconducting mechanism in Fe-based superconductors [20–22]. In this approach, it is quite natural to pay attention to other analogous chalcogenides without iron.

To simplify the potential complex in understanding superconductivity in transition metal chalcogenides, one expects to explore superconductivity in other chalcogenides without magnetic elements. Palladium chalcogenides may offer alternative route for such a purpose. For example, PdTe was found to be a superconductor with a strongly coupled character [34]. By the application of pressure, T_c was theoretically predicated to decrease in this compound [35]. The high-pressure experiments have not been carried out on PdTe yet. However, it is interesting to study the high-pressure behaviors and the evolution of superconductivity with pressure in palladium chalcogenides. So far, many physical properties of this family at high pressures have not been investigated experimentally. Palladium sulfide (PdS) has a wealth of superior physical properties, such as semiconducting, photoelectrochemical, and photovoltaic properties [36–38]. These properties are being developed for device applications in catalysis and acid resistant high-temperature electrodes [39–42]. Recently, this material was identified to be a potential thermoelectric material with large Seebeck coefficient and high electrical conductivity [43]. Pressure has often been used to drive narrow band semiconductors to become superconductors [44, 45]. It is highly desired to examine whether superconductivity can be realized in PdS upon lattice compression and what the path will be undertaken at high pressures.

To address the issues mentioned above, we perform a series of measurements to study the physical properties in PdS under pressure up to 42.3 GPa. We find that the semiconducting behavior is strongly suppressed and a metallic phase develops under pressure from the resistivity measurements. A pressure-induced superconductivity is observed when the phase transition occurs. The phase transition is confirmed by

Raman scattering and x-ray diffraction measurements. The high-pressure phase diagram is thus established for this interesting material.

2. Experimental details

The high-quality sample PdS used in this experiment was synthesized by melting-quenched method and spark plasma sintering, detailed elsewhere [46]. A nonmagnetic diamond anvil cell (DAC) made of Cu–Be alloy was used for high-pressure resistivity measurements [47]. This customized cell has two symmetrical anvil culets with the diameter of 200 μm . An insulated rhenium flake was used as the gasket with the sample chamber of diameter 100 μm . The high-quality PdS was pressed into powders before filled in the sample chamber. A standard four-probe method with four Pt wires linked the sample powers and external Cu wires was used for the resistivity measurements in Physical Properties Measurement System (PPMS). For the Raman scattering experiments, pressure was realized by a symmetrical DAC with a 300 μm culet and the diameter of sample chamber was 150 μm . The sample powers were loaded in the hole with the same conditions for the resistivity measurements. The power of exciting laser was 2 mW with a wavelength of 488 nm, and the integral time was 5 mins in order to obtain better Raman scattering spectra. The high pressure x-ray scattering diffraction experiments, prepared the same environment as Raman measurements, were conducted at the Shanghai Synchrotron Radiation Facility with a wavelength 0.6199 \AA and the size of the x-ray focus beam is less than 2 μm . In all the experiments mentioned above, pressure was calibrated by using the ruby fluorescence shift [48], and the pressure was implemented around room temperature.

3. Results and discussion

Figure 1 shows the temperature dependence of the resistivity for PdS at various pressures up to 41.3 GPa. From figure 1(a), we can see that the resistivity of PdS is strongly suppressed with increasing pressure, and a typical semiconducting feature is observed from the resistivity behavior in all the temperature range at various pressures up to 16.5 GPa. Interestingly, when pressure is increased to 19.6 GPa, it enters into a superconducting state at low temperatures (figure 1(b)). With further increasing pressure, the resistivity is gradually reduced and the superconductivity becomes more evident. This phenomenon can be clearly seen in the enlarged plots of figure 1(e). Moreover, a resistivity hump is observed around 170 K at the pressure of 19.6 GPa. At the same time, a metallic behavior emerges at the normal state of this superconductor below the hump-emerging temperature. This phenomenon indicates an incomplete phase transition from a semiconductor state to a metal state induced by pressure above 19.6 GPa. Upon further compression, the resistivity hump shifts towards to higher temperatures and disappears at the pressure of 30.2 GPa. The origin of the resistivity hump shifting towards to higher temperatures with increasing pressure is derived from the

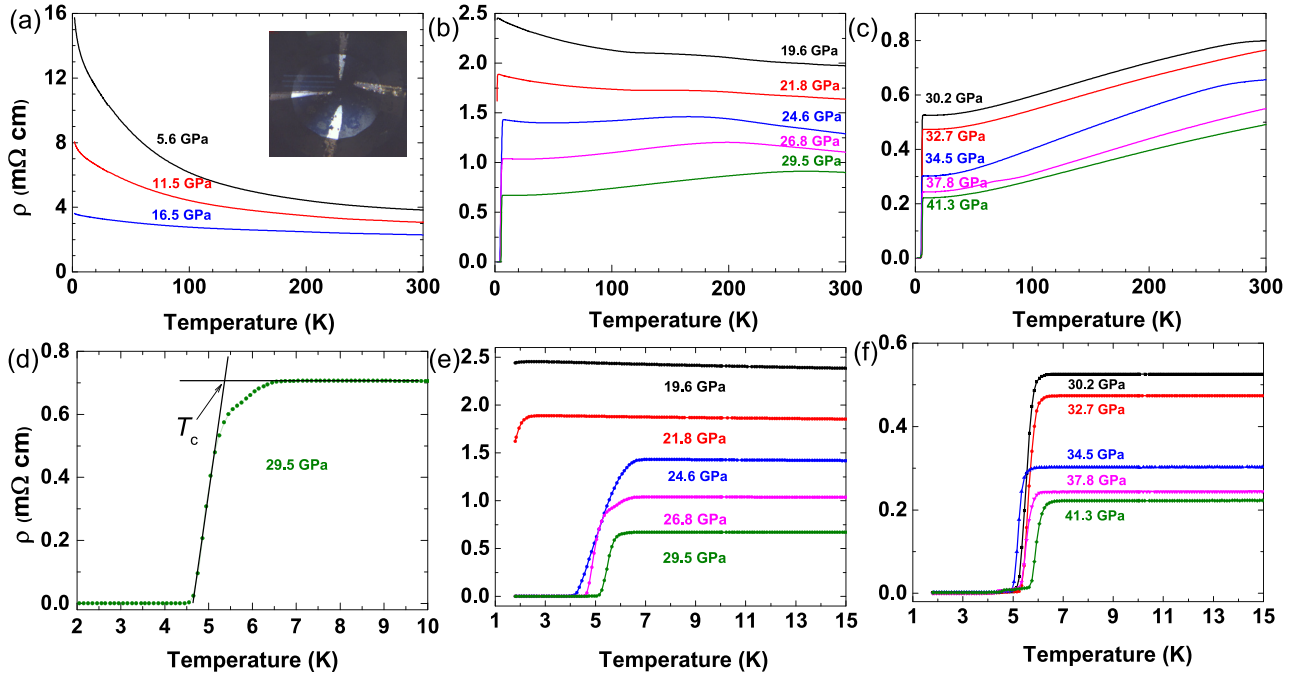


Figure 1. Temperature dependence of the resistivity of PdS at various pressures. (a) The resistivity is gradually suppressed with increasing pressure and behaves like a typical semiconductor. (b) The metallic behaviour gradually becomes dominant with increasing pressure at normal state and superconductivity emerges at 19.6 GPa. (c) The metallic state is fully occupied the crystal at normal state above 30 GPa and superconductivity can be seen obviously. (d) The criterion for determining the T_c , the inset shows the geometry of the probes. (e) and (f) are the enlarged plots showing the transitions for the corresponding panels of (b) and (c).

competing of these two phases. As shown in figure 1(c), the semiconducting state disappears and the metallic state occupies the normal state above 30.2 GPa. At 41.3 GPa, the highest pressure studied in this article, superconductivity is still persisting with an improved T_c which can be clearly seen in figure 1(f). These results suggest that a new superconductor is discovered at high pressures, which may be accompanied by the structural phase transition.

The emergence of superconductivity is confirmed by the measurements of temperature dependence of the resistivity at different magnetic fields. The results at the pressure of 29.5 GPa are summarized in figure 2. It can be seen that the temperature dependent resistivity curve gradually shifts towards the low temperatures with increasing magnetic fields. Finally, the the temperature dependent resistivity almost becomes flat between 1.8 and 10 K with the magnetic field of 4.5 T, which indicates the complete suppression of superconductivity in PdS. These magnetic-field dependent measurements provide convincing evidence for the detected superconducting transition at high pressures. Within the weak-coupling Bardeen–Cooper–Schrieffer (BCS) theory, an upper critical field at $T = 0$ K can be determined by the Werthamer–Helfand–Hohenberg equation [49]: $H_{c2}(0) = 0.693[-(dH_{c2}/dT)]_{T_c} T_c$. The calculated $H_{c2}(0)$ is about 5.5 T. The colorful area shown in the inset of figure 2 is the fitted temperature dependence of H_{c2} with the expression: $H_{c2}(T) = H_{c2}(0)[1 - (T/T_c)^2]/[1 + (T/T_c)^2]$ based on the Ginzburg–Landau theory [50].

In order to shed insight into the origin of superconductivity in PdS at high pressures, the Raman scattering measurements were performed at the same condition as resistivity measurements. As we known, Raman spectroscopy can provide

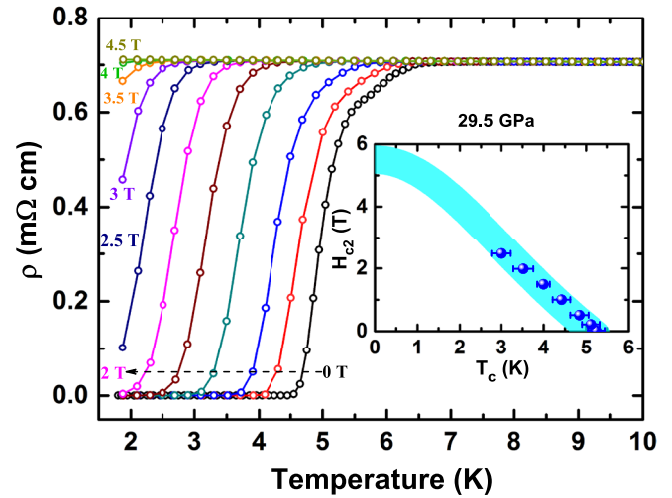


Figure 2. Temperature dependence of the resistivity of PdS at a pressure of 29.8 GPa with applied magnetic fields. Inset: Upper critical field H_{c2} at the pressure of 29.8 GPa. The color area represents the calculated H_{c2} from the Werthamer–Helfand–Hohenberg equation.

valuable information on the lattice vibration. Thus, it is a powerful tool to probe the structural evolution and phase transition. The selected room temperature Raman spectra of PdS at various pressures up to 42.3 GPa are shown in figures 3(a) and (b). To clarity, the obtained Raman vibration modes are marked by arrows and denoted as L_m , respectively. Upon increasing pressure, most of the obtained Raman modes are broad at low pressures, indicating a strong electron–phonon coupling and phonon–phonon interaction. Above 16.2 GPa, the Raman mode L_4 is disappearing which indicates the appearance of a

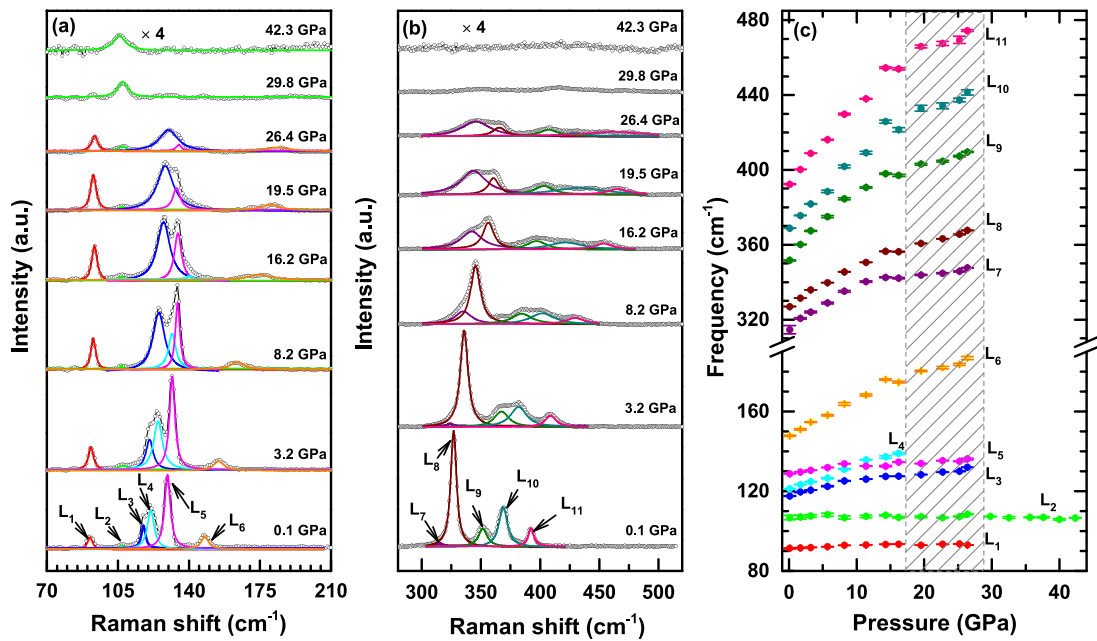


Figure 3. Selected Raman spectra of PdS at room temperature and various pressures in the ranges of (a) 70–210 cm^{-1} and (b) 280–520 cm^{-1} . (c) Pressure dependence of the obtained phonon frequencies. The dashed region is the transition area and represents the coexistence of two phases.

new high-pressure phase. In other words, the sample PdS has evolved into a coexistence of two phases including the initial phase (tetragonal structure) and a new phase (the metallic phase). This is consistent with the emerging of superconductivity from the resistivity measurements (figure 1(b)). With further increasing pressure, the gradually weakened intensity of the Raman modes is consistent with the gradually obvious metallic normal state (figure 1(b)). Above 29.8 GPa, almost all the Raman modes disappear excepting the very weak and broad L_2 , indicating that the sample PdS completely evolved into the metallic phase as shown in figure 1(b).

Depending on the Lorentzian fitting [51], the pressure dependence of the obtained phonon frequencies are shown in figure 3(c). It is obvious that PdS undergoes a phase transition in the intermediary areas and the dashed area in a rough range between 16.2 and 29.8 GPa represents the coexistence of two phases. Almost all the Raman modes shift toward higher frequencies obviously under pressure before 19.6 GPa, originating from the expected contraction of interatomic distances. However, all the vibrational mode do not change too much between the coexisted phases. Above 26.5 GPa, only the vibrational mode L_2 ($\times 4$) is still existing. Thus, the vibrational mode L_2 may be special to the strong electron–phonon coupling in favor of superconductivity.

Generally speaking, a sharp reduction of Raman peaks can be attributed to a structure transton with high symmetry where no Raman mode is allowed, or because of a transition to a metallic state which will shield the Raman signal due to the limited penetration depth of the exciting laser. In order to give a well-established evidence to the structure evolution in PdS, room-temperature synchrotron x-ray diffraction patterns of PdS at various pressures are measured up to 45.8 GPa. As shown in figure 4, all the Bragg peaks shift to larger angles with the increase of pressure, showing the shrinkage of the

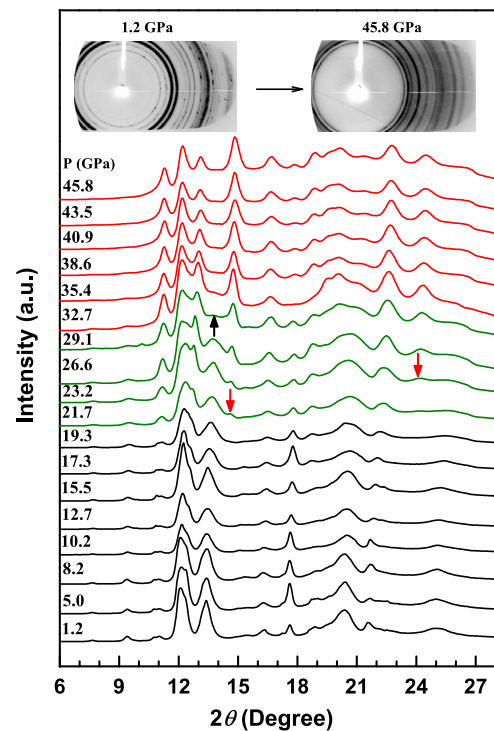


Figure 4. High-pressure synchrotron x-ray diffraction patterns of PdS. The disappeared and emerging peaks are marked by black and red arrows, respectively. The original diffraction patterns (1.2 GPa and 45.8 GPa) are shown on the top.

PdS lattice. Almost all diffraction peaks can be fitted to the tetragonal symmetry at low pressure, suggesting that the crystal structure of the PdS is stable below 19 GPa. Upon further compression, a new peak marked by a red arrow appears at 21.7 GPa, which means that a new phase emerges. Then, another new peak which is also marked by a red arrow appears

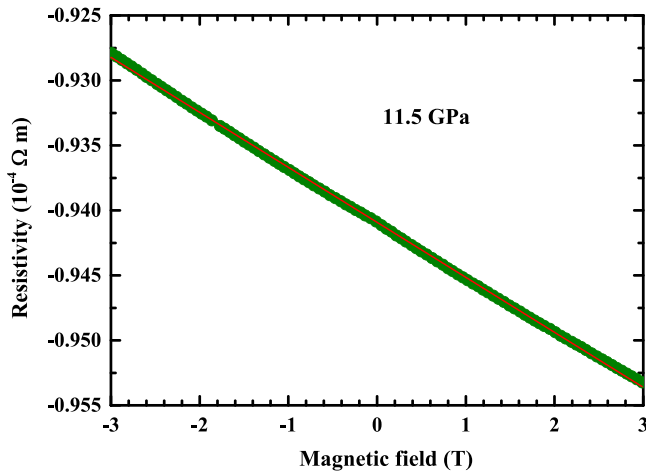


Figure 5. Magnetic field dependence of the Hall resistivity measured at 10 K under the pressure of 11.5 GPa.

at 23.2 GPa. And these two new peaks become more evident with further increasing pressure. On the contrary, the Bragg peak marked by a black arrow disappears at the pressure of 29.1 GPa. These results suggest that the two phases coexist between 21.7 and 29.1 GPa, which is consistent with the resistivity and Raman scattering measurements. Above 32.7 GPa, the material completely evolves into the new phase revealed by Raman spectra. The new phase is a more complex phase, which is also supported by the original diffraction patterns on the top of figure 4. The details of the new structure are still under investigation. However, it is certain that pressure drives PdS to evolve into a more complex structural phase above 19.5 GPa.

The phase diagram of PdS is mapped out by combining the resistivity, Raman scattering, and x-ray diffraction measurements (figure 6). It can be seen that PdS keeps its initial phase with the behavior as a semiconductor (S) under the pressure of 19.5 GPa. Then, with increasing pressure, it evolves into a superconducting state with the coexistence of two phases between 19.5 and 29.8 GPa. It is specially interesting that T_c has an obvious improvement in the region of the coexisted phases. With a roughly linear fitting (red-dot line), the initial pressure dependent coefficient of T_c , dT_c/dP (about 0.58 K GPa^{-1}) is obtained. After the obvious improvement, T_c is observed to level off with increasing pressure together with a complete evolution into a metallic (M) state at normal state. Overall, T_c first exhibits a arc-like shape with increasing pressure and then becomes almost constant upon heavy compression. This behavior is very similar to a reported superconductor (NbN), where T_c roughly increases with applied pressure up to 4 GPa, and then reaches a constant from 4 GPa to 42 GPa [52].

The lower panel of figure 6 shows the pressure dependence of Hall coefficient (R_H) and carrier concentration. The R_H can be obtained by using a linear fitting to the data of magnetic field dependent Hall resistivity. A representative Hall setup at 11.5 GPa has been shown in figure 5. The applied fields for the Hall measurements are from -3 to 3 T. The carrier concentration is calculated through the formula $n = 1/eR_H$, where e is the unit of the charge. The negative R_H demonstrates that the

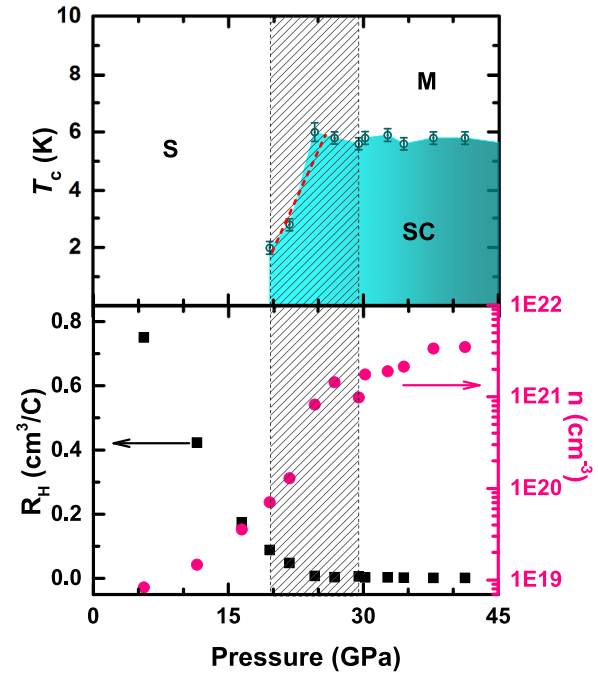


Figure 6. Phase diagram of PdS at high pressures. The red-dot line is a linear fitting for dT_c/dP . The lower panel shows the pressure dependence of the Hall coefficient and carrier concentration measured at 10 K. The dashed region represent the phase borders of a semiconductor (S) and metal (M). The dashed area represents the coexistence of two phases.

dominant electron carrier character for the superconducting phase. The sign of the calculated carrier concentration at 10 K gradually increases with increasing pressure in initial phase region. Then, the carrier concentration has a relatively weak pressure dependence at higher pressures after a noticeable rise in the region of the coexisted phases. The carrier concentration for the superconducting phase is in the range between 10^{20} and 10^{22} cm^{-3} , at least two order higher in magnitude than that at ambient condition, which is very beneficial to the electron–phonon coupling in favor of superconductivity. The pressure dependent T_c and evolution of carrier concentration under pressure are coherent, especially the obvious increase of them around the same pressure range. This phenomenon may have provided a natural explanation for the superconductivity of PdS under pressure.

The properties of conventional superconductors can be explained well by the theory of BCS, and the superconductivity is always driven from the coupling between electrons and phonons (lattice vibrations) [53]. Recently, the strong electron–phonon interaction has been observed in transition metal chalcogenides, which indicates the importance of electron–phonon coupling for high temperature superconductivity [32, 33, 54, 55]. PdS as a transition metal chalcogenide, should be also an electron–phonon coupled superconductor.

For phonon-mediated superconductivity, T_c can be expressed as $T_c \propto \langle \omega_{\text{log}} \rangle \exp[-1.04(1 + \lambda)/\lambda]$ [56, 57]. Here, the electron–phonon coupling constant λ is determined by the equation of $\lambda = \frac{N(0)\langle I^2 \rangle}{M\langle \omega^2 \rangle}$, where $\langle \omega_{\text{log}} \rangle$ is phonon energy, $N(0)$ is the density of electronic states at the Fermi energy, $\langle I^2 \rangle$ is

the mean-square electron–phonon matrix element, M is the ionic mass, and $\langle\omega^2\rangle$ is the mean-square frequencies over the phonon spectra. Previous studies have established that $\langle I^2\rangle$ and M do not change too much with pressure [52, 58]. The information about phonon energy could be estimated from the Raman spectra (figure 3). In the superconducting regime, the phonon energy $\langle\omega_{\text{log}}\rangle$ and $\langle\omega^2\rangle$ are not sensitive to pressure. The electronic part of λ could be reflected by carrier concentration which is proximate to $N(0)$ (figure 6). It is obvious that the pressure dependence T_c and carrier concentration is synchronous in the superconducting regime. Combined with the relationship of T_c and λ , there is no doubt that the electron–phonon pairing mechanism plays an important role in superconductivity of PdS.

4. Conclusions

In summary, we have synthesized high-quality sample PdS with single phase at ambient pressure. High-pressure resistivity, Hall coefficient, Raman scattering, and x-ray diffraction measurements have been performed on PdS up to 42.3 GPa. With increasing pressure, the semiconducting behavior has been strongly suppressed. A metallic phase has emerged and gradually occupied the dominant position upon further compression. The pressure-driven semiconductor-metal transition has been examined by combining Raman scattering and x-ray diffraction. Superconductivity has been observed when the metallic phase emerges at pressure of 19.6 GPa. The character of superconductivity has been confirmed by the obtained zero resistance and the suppression of the resistivity with the application of magnetic fields. We suggested that the evolution of T_c under pressure was dominated by the carrier concentration. These findings enrich the superconducting family from transition metal chalcogenides. PdS-derived superconductors with higher T_c are expected under pressure. These results will shed new light on understanding the mechanism of superconductivity in this kind of materials.

Acknowledgments

Lei Su acknowledges the support from the Natural Science Foundation of China (No. 21273206). Xun Shi and Li-Dong Chen acknowledges the support from the National Basic Research Program of China (973-program) under Project No. 2013CB632501, the Natural Science Foundation of China under No. 11234012, and the Shanghai Government (Grant No.15JC1400301).

ORCID iDs

Liu-Cheng Chen  <https://orcid.org/0000-0002-8066-2789>

References

- [1] Kamihara Y, Watanabe T, Hirano M and Hosono H 2008 *J. Am. Chem. Soc.* **130** 3296
- [2] Chen X H, Wu T, Wu G, Liu R H, Chen H and Fang D F 2008 *Nature* **453** 761
- [3] Shi H L, Yang H X, Tian H F, Lu J B, Wang Z W, Qin Y B, Song Y J and Li J Q 2010 *J. Phys.: Condens. Matter* **22** 1257002
- [4] Jeevan H S, Hossain Z, Kasinathan D, Rosner H, Geibel C and Gegenwart P 2008 *Phys. Rev. B* **78** 092406
- [5] Glasbrenner J K, Mazin I I, Jeschke H O, Hirschfeld P J, Fernandes R M and Valenti R 2015 *Nat. Phys.* **11** 953
- [6] Fernandes R M, Chubukov A V and Schmalian J 2014 *Nat. Phys.* **10** 97
- [7] Abdel-Hafiez M *et al* 2015 *Phys. Rev. B* **91** 165109
- [8] Wang Q S *et al* 2016 *Nat. Commun.* **7** 12182
- [9] Wang Q S *et al* 2016 *Nat. Mater.* **15** 159
- [10] Luo C W *et al* 2012 *Phys. Rev. Lett.* **108** 257006
- [11] Diko P, Antal V, Kavecansky V, Yang C and Chen I 2012 *Physica C* **476** 29
- [12] Wang F, Kivelson S A and Lee D H 2015 *Nat. Phys.* **11** 959
- [13] Cao H Y, Chen S, Xiang H and Gong X G 2015 *Phys. Rev. B* **91** 020504
- [14] Hsu F C *et al* 2008 *Proc. Natl Acad. Sci.* **105** 14262
- [15] Medvedev S *et al* 2009 *Nat. Mater.* **8** 630
- [16] Devey A J, Grau-Crespo R and Leeuw N H 2008 *J. Phys. Chem. C* **29** 10960
- [17] Kwon K D, Refson K, Bone S, Qiao R M, Yang W L, Liu Z and Sposito G 2011 *Phys. Rev. B* **83** 064402
- [18] Lai X F, Zhang H, Wang Y Q, Wang X, Zhang X, Lin J H and Huang F Q 2015 *J. Am. Chem. Soc.* **32** 10148
- [19] Lai X F, Liu Y, Lü X J, Zhang S J, Bu K J, Jin C Q, Zhang H, Lin J H and Huang F Q 2016 *Sci. Rep.* **6** 31077
- [20] Mizuguchi Y, Tomioka F, Tsuda S, Yamaguchi T and Takano Y 2008 *Physica C* **469** 1027
- [21] Subedi A, Zhang L J, Singh D J and Du M H 2008 *Phys. Rev. B* **78** 134514
- [22] Maheshwari P K, Jha R, Gahtori B and Awana V P S 2015 *J. Supercond. Novel Magn.* **28** 2893
- [23] Millican J N, Phelan D, Thomas E L, Leão J B and Carpenter E 2009 *Solid State Commun.* **149** 707
- [24] Garbarino G, Sow A, Lejay P, Sulpice A, Toulemonde P, Mezouar M and Núñez-Regueiro M 2009 *Europhys. Lett.* **86** 27001
- [25] Tissen V G, Ponyatovsky E G, Nefedova M V, Titov A N and Fedorenko V V 2009 *Phys. Rev. B* **80** 092507
- [26] Braithwaite D, Salce B, Lapertot G, Bourdarot F, Marin C, Aoki D and Hanfland M 2009 *J. Phys.: Condens. Matter* **21** 232202
- [27] Miyoshi K, Takaichi Y, Mutou E, Fujiwara K and Takeuchi J 2009 *Japan. J. Phys. Soc.* **78** 093703
- [28] Margadonna S, Takabayashi Y, Ohishi Y, Mizuguchi Y, Takano Y, Kagayama T, Nakagawa T, Takata M and Prassides K 2009 *Phys. Rev. B* **80** 064506
- [29] Kumar R S, Zhang Y, Sinogeikin S, Xiao Y, Kumar S, Chow P, Cornelius A L and Chen C F 2010 *J. Phys. Chem. B* **114** 12597
- [30] Imai T, Ahilan K, Ning F L, McQueen T M and Cava R J 2009 *Phys. Rev. Lett.* **102** 177005
- [31] Marty K *et al* 2012 *Phys. Rev. B* **86** 220509
- [32] Mandal S, Cohen R E and Haule K 2014 *Phys. Rev. B* **89** 220502
- [33] Gerber S *et al* 2017 *Science* **357** 71
- [34] Karki A B, Browne D A, Stadler S, Li J and Jin R 2012 *J. Phys.: Condens. Matter* **24** 055701
- [35] Chen J and Wang X 2016 *Solid State Sci.* **52** 23
- [36] Ferrer I J, Chao P D, Pascual A and Sánchez C 2007 *Thin Solid Films* **515** 5783
- [37] Folmer J C W, Turner J A and Parkinson B A 1987 *J. Solid State Chem.* **68** 28
- [38] Barawi M, Ferrer I J, Ares J R and Sánchez C 2014 *ACS Appl. Mater. Interfaces* **6** 20544

- [39] Bladon J J, Lamola A, Lytle F W, Sonnenberg W, Robinson J N and Philipose G 1996 *J. Electrochem. Soc.* **143** 1206
- [40] Alan J M, Antonio G R, Inmaculada R M and James A A 2016 *J. Catal.* **340** 10
- [41] Yang C H, Wang Y Y, Wan C C and Chen C J 1996 *J. Electrochem. Soc.* **143** 3521
- [42] Zubkov A, Fujino T, Sato N and Yamada K 1998 *J. Chem. Thermodyn.* **30** 571
- [43] Chen L C, Jiang B B, Yu H, Pang H J, Su L, Shi X, Chen L D and Chen X J 2018 Thermoelectric properties of polycrystalline palladium sulfide (arXiv:1802.02761)
- [44] Ying J J, Struzhkin V V, Cao Z Y, Goncharov A F, Mao H K, Chen F, Chen X H, Gavriluk A G and Chen X J 2016 *Phys. Rev. B* **93** 100504
- [45] Chen X J, Zhang C, Meng Y, Zhang R Q, Lin H Q, Struzhkin V V and Mao H K 2011 *Phys. Rev. Lett.* **106** 135502
- [46] Li X Y, Li D, Xin H X, Zhang J, Song C J and Qin X Y 2013 *J. Alloys Compd.* **561** 105
- [47] Gavriluk A G, Mironovich A A and Struzhkin V V 2009 *Rev. Sci. Instrum.* **80** 043906
- [48] Mao H K, Bell P M, Shaner J W and Stembey D J 1978 *J. Appl. Phys.* **49** 3276
- [49] Werthamer N R, Helfand E and Hohenberg P C 1966 *Phys. Rev.* **147** 295
- [50] Ni N, Tillman M E, Yan J Q, Kracher A, Hannahs S T, Bud'ko S L and Canfield P C 2008 *Phys. Rev. B* **78** 214515
- [51] Singh R K, Singh S N, Asthana B P and Pathak C M 1994 *J. Raman Spectrosc.* **25** 423
- [52] Chen X J, Struzhkin V V, Wu Z G, Cohen R E, Kung S, Mao H K, Hemley R J and Christensen A N 2005 *Phys. Rev. B* **72** 094514
- [53] Bardeen J, Cooper L N and Schrieffer J R 1957 *Phys. Rev.* **108** 1175
- [54] Lanzara A *et al* 2001 *Nature* **412** 510
- [55] Koufos A P, Papaconstantopoulos D A and Mehl M J 2014 *Phys. Rev. B* **89** 035150
- [56] McMillan W L 1968 *Phys. Rev.* **167** 331
- [57] Ekimov E A, Sidorov V A, Bauer E D, Mel'nik N N, Curro N J, Thompson J D and Stishov S M 2004 *Nat. Lett.* **428** 542
- [58] Chen X J, Struzhkin V V, Kung S, Mao H K, Hemley R J and Christensen A N 2004 *Phys. Rev. B* **70** 014501